J Nanopart Res (2012) 14:951
DOI 10.1007/s11051-012-0951-0

REVIEW

Ionic transport in nanocapillary membrane systems

Vikhram V. Swaminathan · Larry R. Gibson II · Marie Pinti · Shaurya Prakash · Paul W. Bohn · Mark A. Shannon

Received: 11 March 2012 / Accepted: 23 May 2012

Abstract Species transport in nanocapillary membrane systems has engaged considerable research interest, presenting technological challenges and opportunities, while exhibiting significant deviations from conventionally well understood bulk behavior in microfluidics. Nonlinear electrokinetic effects and surface charge of materials, along with geometric considerations, dominate the phenomena in structures with characteristic lengths below 100 nm. Consequently, these methods have enabled 3D micro- and nanofluidic hybrid systems with high-chemical selectivity for precise manipulation of mass-limited quantities of analytes. In this review, we present an overview of both fundamental developments and applications of these unique nanocapillary systems, identifying forces that govern ion and particle transport, and surveying applications in separation, sensing, mixing, and chemical reactions. All of these developments are oriented toward adding important functionality in micro-total analysis systems.

Keywords Membranes · Nanostructures · Nanofluidics · Microfluidics · Ion transport · Electrokinetics · μ-TAS · Nanopore · Nanocapillary · Water filtration · Sustainable development

Special Issue Editors: Mamadou Diallo, Neil Fromer, Myung S. Jhon

This article is part of the Topical Collection on Nanotechnology for Sustainable Development

Introduction

The development of nanofluidic systems containing nanocapillary array membranes (NCAMs) is strongly motivated by the interesting phenomena that occur at length scales between 1 and 100 nm. NCAMs consist

V. V. Swaminathan · M. A. Shannon (✉)
Department of Mechanical Science and Engineering, University of Illinois at Urbana-Champaign, Urbana, IL 61801, USA
e-mail: mshannon@illinois.edu

L. R. Gibson II · P. W. Bohn
Department of Chemical and Biomolecular Engineering, University of Notre Dame, Notre Dame, IN 46556, USA

M. Pinti · S. Prakash
Department of Mechanical and Aerospace Engineering, The Ohio State University, Columbus, OH 43210, USA

P. W. Bohn
Department of Chemistry and Biochemistry, University of Notre Dame, Notre Dame, IN 46556, USA

M. A. Shannon
Department of Chemical and Biomolecular Engineering, University of Illinois at Urbana-Champaign, Urbana, IL 61801, USA

Published online: 04 July 2012

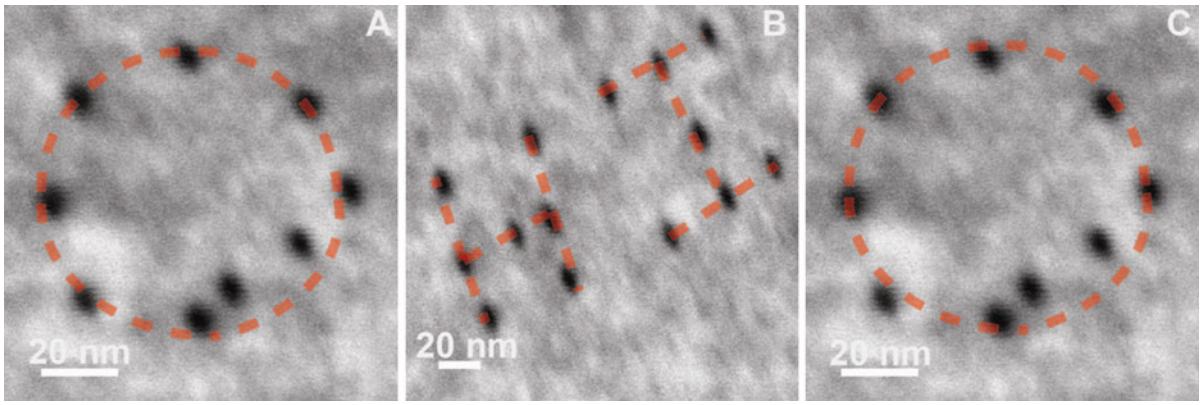

Fig. 1 Fabrication of nanopore arrays using a transmission electron microscope (TEM). Ordered arrangements were fabricated to illustrate the word "OHIO" with elliptical cross-section nanopores. The *red-dotted line* is meant to serve as an eye-guide. The pores in **a** and **c** are 4 ± 0.4 x 2.6 ± 0.6 nm The nanopores that spell out "H" and "I" are 5.8 ± 0.7 x 3.0 ± 0.5 nm as shown in **b**. This figure is taken from Prakash et al. 2012

of monodisperse nanopores fabricated in a polymer membrane, most commonly composed of polycarbonate sheets with thickness on the order of 6–10 μm, with nanopores produced from the damage tracks created by high-energy (∼2 MeV) alpha particles, followed by chemical etching to produce nanopores ranging in diameter from 10 to 800 nm. These NCAMs are commercially available. Next generation NCAMs are fabricated with various geometries, in different polymers and in multi-lamellar structures. For example, fabrication of solid-state nanopores similar to NCAMs with a transmission electron microscope has been achieved in silicon nitride membranes with controlled cross-section geometry and ordered arrangement of the nanopores (Prakash et al. 2012a, b) (Fig. 1).

The influence of surface charge, surface potentials, and subsequent electrostatic forces lead to hindered transport, selectivity, and partitioning of chemical and biological species. Such systems draw advantage from enhanced surface area-to-volume (SA/V) scaling that leads to reduced diffusion time scales in contrast to conventional microfluidic systems for transport toward surfaces and rapid kinetics. The ability to capture and manipulate extremely small quantities of analytes (zeptoliter to attoliter volumes) with high precision and flexibility approaching the molecular level, and to execute multiple analytical unit operations on-chip, has strongly driven several fundamental studies and applications of separation, concentration, and sensing systems aimed toward developing better tools of chemical analysis and biological diagnostics.

In recent years, numerous articles have reviewed concepts of nanofluidic transport phenomena and their applications in chemical and biological analysis, (Han et al. 2008; Schoch et al. 2008; Prakash et al. 2008, 2009; Sparreboom et al. 2009; Bohn 2009; Piruska et al. 2010a, b; Mulero et al. 2010). Technological advancements in micro- and nanofabrication have facilitated the realization of systems integrated with nanocapillary arrays in microfluidic devices, and methods of surface modification of pore surfaces (Nishizawa et al. 1995) have enabled excellent control and modulation of factors governing nanoscale transport. The purpose of this review is to present a broad overview of nanoscale transport phenomena in NCAMs, highlighting outcomes of fundamental studies, along with advancements in a variety of application areas.

Background

Flow characteristics through nanostructures such as nanopores, NCAMs, nanochannels, and nanotubes are largely determined by the size, geometry, and surface chemistry (i.e., surface charge density and surface energy) of the nanostructure. The characteristic dimension of a nanocapillary is its pore diameter, a, which lies typically in the range of 1–100 nm for nanofluidic phenomena. The Debye length, λ_D, is a critical scaling parameter that captures the extent of surface charge shielding in nanoscale geometries. As physical feature dimensions approach this value new phenomena such as perm selectivity (Nishizawa et al. 1995) come into play

with the primary driving forces for transport being electrokinetic flow or surface mediated transport (Prakash et al. 2008). While this condition can intersect with the transition between continuum and molecular models, it can be used to address individual molecules (Bohn 2009). On one hand, fluid dynamics within high-aspect ratio nanocapillaries is beset with size effects—shielding and apparent electro viscosity that lead to hindered transport. However, surfaces and their characteristic properties such as charge and potential distributions determine the environment and forces experienced by ions and cause effects of selectivity and partitioning.

Transport equations in cylindrical capillaries

Even though the basis for most modern-day electrokinetics arises from colloidal theories developed well over 100 years ago, detailed analytical studies of electrokinetic flow in fine capillaries date back to 1964, where it was demonstrated for rectangular slit geometries that, for large values of the surface potential, Ψ_0, and sufficiently small κa, where κ equals $1/\lambda_D$, electrokinetic retardation effects opposed pressure-induced flow when capillary dimensions shrink down to 100 nm (Burgreen and Nakache 1964). Rice and Whitehead derived the analytical solution to the potential distribution, Ψ, inside a cylindrical capillary, for small surface potential, Ψ_0, using a Poisson-Boltzmann distribution equation (Rice and Whitehead 1965)

$$\frac{1}{r}\frac{\partial}{\partial r}\left(r\frac{\partial \psi}{\partial r}\right) = \kappa^2\psi, \tag{1}$$

where

$$\kappa = \sqrt{\frac{8\pi n e^2}{\varepsilon kT}}, \tag{2}$$

with n representing the bulk concentration of ions per unit volume, e is the fundamental charge, ε is the electrical permittivity, k is the Boltzmann's constant, and T is the temperature. The solution for potential distribution follows

$$\psi = \psi_0 \frac{I_0(\kappa r)}{I_0(\kappa a)}, \tag{3}$$

where I_0 is the modified Bessel equation of the first kind. This analytical solution was valid to within 3 % accuracy for small values of $\Psi_0 < kT \approx 25$ mV, and later extended up to 50 mV based on asymptotic approximations. Combining this with the steady-state Navier–Stokes' equation for fluid motion

$$\eta\nabla^2 v + (v\cdot\nabla)v + \nabla p = F, \tag{4}$$

where η is the viscosity, p is the pressure, and F is the body force, yields the electroosmotic velocity, $v(r)$, as follows

$$v(r) = \frac{a^2 - r^2}{4\eta}p_z - \Omega E_z\left[1 - \frac{I_0(\kappa r)}{I_0(\kappa a)}\right], \tag{5}$$

where $\Omega = \dfrac{\varepsilon\psi}{4\pi\eta}$, and E_z is the axial electric field that represents the body force.

Advanced computational techniques and molecular dynamics simulations have been incorporated to validate analytical and numerical models for ionic transport (Conlisk et al. 2002; Qiao and Aluru 2003; Conlisk 2005). Furthermore, the effects of surface charge/wall potentials, ionic size, and differential transport on electroosmotic flow (EOF) in nanochannels and membranes have been studied both computationally (Qiao and Aluru 2004; Qiao et al. 2006; Conlisk et al. 2007) and experimentally (Sadr et al. 2006).

The local potential distribution shown in Eq. 3 is strongly dependent on length scales and Fig. 2 shows schematic profiles for different values of κa with a more detailed discussion found in several textbooks (Conlisk 2012) and recent reviews (Prakash et al. 2012a, b). When pores are sufficiently large, or the ionic strength is large and membrane potential small, so that κa >> 1 (Fig. 2a), the electrochemical double layers (EDLs) are compact and the core region of the

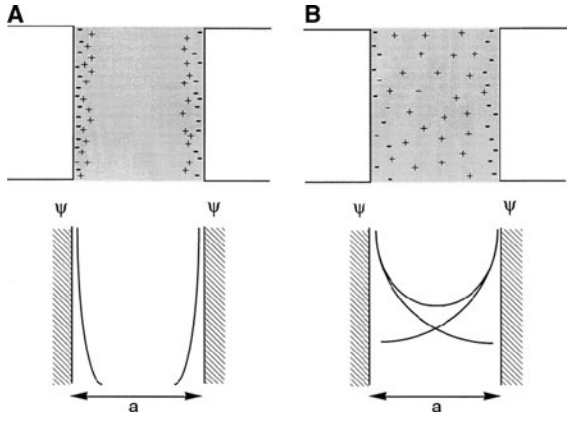

Fig. 2 Schematic representation of the formation of the EDLs and potential profiles within nanopores at the extreme conditions where **a** κa >> 1 when the EDLs are compact and **b** κa $\leq$ 1 when the EDLs overlap and lead to permselectivity. Reprinted with permission, (Kemery et al. 1998). Copyright 1998 American Chemical Society

pore retains bulk-like concentration and plug-flow electrophoretic characteristics (Kemery et al. 1998). On the other hand, narrow pores with dilute media, corresponding to $\kappa a \leq 1$, form overlapped EDLs with radial velocity following Poiseuille flow-like parabolic characteristic. Consequently, counter-ions are drawn into the pore and co-ions rejected to maintain charge neutrality (Fig. 2b), and give rise to perm selectivity by the exclusion-enrichment effect (Plecis et al. 2005). Local asymmetry in solute distribution causes deviations from bulk electrostatic behavior—most notably, the EOF arising from interactions with the wall charge dominating over electrophoresis.

The electroviscous effect and enhanced conductivity

At length scales of $\kappa a \leq 10$, it has been estimated through flow-rate measurements fit to conventional Poiseuille flow that the apparent viscosity is enhanced over that of Poiseuille flow due to back flow from EOF effects. The resulting enhanced viscosity is often referred to as electroviscosity since surface charge has been shown to cause increased structuring or layering of water near the pore walls through molecular dynamics simulations (Qiao and Aluru 2003). Further in the case of nanopores, when $\kappa a \leq 1$, interacting double layers cause decreased solvent flow and may also contribute to the apparent viscosity. Huisman et al. (2000) calculated the electroviscous effect from measurements of streaming potential and showed that differences in ionic mobilities in binary electrolytes broke zeta potential (ζ-potential) symmetry and enhanced the electroviscosity. A Knudsen number based on the ratio of molecular interaction length over system characteristic dimension has been suggested for modeling fluidic resistance under Stokes' flow in nanochannels (Sparreboom et al. 2010). Backflow of ions under the electric field arising from electroosmotic pressure is also enhanced by the surface conductance, G_s, due to the presence of the EDLs, and contributes to increased conductivity of the electrolyte inside the pore, λ_{pore}, than in bulk, λ_{bulk}, such that

$$\lambda_{\text{pore}} = \lambda_{\text{bulk}} + \frac{2G_s}{a}. \tag{6}$$

It should be noted here that electroviscosity is an effect that has been used to explain deviations from conventional theory, and some molecular dynamics simulations have shown fluid layering as one possible reason for enhanced viscosity, but independent experimental verification of increased fluid viscosity have not yet been reported.

Streaming potential

The streaming potential, a measurable quantity, serves as a useful experimental tool used in gauging separation performance of ultrafiltration (UF) and nanofiltration (NF) membranes (Nystrom et al. 1989; Agerbaek and Keiding 1995; Fievet et al. 2000; Datta et al. 2010). Surface charge of membranes is often characterized using ζ-potential at slip planes derived from streaming potential measurements. Experimentally determined ζ-potentials in both aqueous and non-aqueous media (Chowdiah et al. 1983) substantially exceeded the calculations from Helmholtz–Smoluchowski theory using analytical correction factors (Rice and Whitehead 1965). Nystrom and colleagues reported a 10-fold increase in apparent ζ-potentials when correction factors and the influence of membrane surface charge and double layer were suitably taken into account. In pH-dependent transport experiments of chlorolignin through polyvinylidene fluoride (PVDF) UF membranes, strong electrostatic repulsions were observed when the polyelectrolyte was fully dissociated, whereas neutral molecules passed through when they were un-dissociated at a low pH of 3. Determining a true ζ-potential from experimental measurements required extending Rice and Whitehead's model to account for larger pore potentials by numerical calculations using the space-charge model (Szymczyk et al. 1999). Especially in the case of nanocapillary membranes with hydrophilic surfaces, the strong coupling between transport phenomena presents a hard challenge for the measurement of ζ-potential with overlapped EDLs. Furthermore, in the case of overlapped EDLs, the notion of slip planes and hence ζ-potential loses physical significance (Prakash et al. 2008).

Transport of macromolecules

Besides the effect of capillary size and λ_D, a third length scale, based on the ionic size, R_i, affects transport characteristics of NCAMs. Incorporating the

finite size of ions, particularly for systems with $\kappa a \sim 1$, was found to have significant effect in suppressing average ionic concentrations and electrical conductance inside pores while increasing selectivity and streaming potential (Cervera et al. 2010). The Renkin equation (Renkin 1954) captures the effect of ionic size relative to pore radius in decreased species diffusion coefficient, D_i, within a confined pore in comparison with bulk values, D_0, such that

$$D_i = D_0\left[1 - 2.104\frac{R_i}{a} + 2.09\left(\frac{R_i}{a}\right)^2 - 0.95\left(\frac{R_i}{a}\right)^5\right]. \quad (7)$$

Studies of peptide concentration using NCAMs (Zhang and Timperman 2003) and, more recently, protein dynamics in silicon nitride nanopores have clearly demonstrated the hindered macromolecular transport effect (Oukhaled et al. 2011). Dwell-times measured for proteins were found to be on the order of milliseconds while diffusion-based calculations predicted microsecond timescales, which is attributed to the protein-wall adsorption interactions as well as EOF retardation. Further, anomalous protein dynamics in nanopores, including longer dwell-times for compact proteins than those of unfolded structures, are indicative of entropic energy costs associated with size, unfolding, and interactions of heterogeneous charge macromolecule structures with nanocapillary surfaces (Talaga and Li 2009; Napoli et al. 2010) that are not yet fully understood.

Transport studies at NCAM-microchannel interfaces

One of the challenges in microfluidics (and even more so in nanofluidics) is the ability to provide controlled metering of fluid and chemical or biological species for specific unit operations. The interface between microchannels and NCAMs can lead to strong discontinuity in electrokinetic characteristics, and various parameters—pore size, pH, ionic strength, and functionality—can be used to control and regulate molecular transport. Kuo et al. (2001), investigated these effects on flux through NCAMs with both hydrophobic and hydrophilic surfaces. In high-ionic strength, diffusion dominated the transport in hydrophilic membranes while hydrophobic membranes were controlled by ion migration. Transport direction could be reversed, under the same applied electric field, by modifying surface charge or ionic strength. At low-ionic strength, EOF effects dominated transport as surface charge determined the direction, with pH acting as a fine-tuning parameter. The choice of many control variables enables a high degree of control over nanofluidic gated injections, a powerful strategy capable of enhancing several applications discussed in section 5.

Molecular gating

Molecular gating refers to the selective transport of ions or molecules based on electrical interactions with an externally applied potential and the surface charge of the NCAM. The ion gating concept was studied as early as 1982 with the use of embedded electrodes and redox polymer membranes in a macroporous system (Burgmayer and Murray 1982). The device depicted in Fig. 3 consists of an NCAM placed between two polydimethylsiloxane (PDMS) microfluidic channels and is used to illustrate the way selection of properties such as pore size and surface chemistry allow for electrically biased flow manipulation within the device (Kuo et al. 2003a, b). An applied potential between the source and receiving channels drives the flow, with forward bias defined as the configuration that causes depletion in the source channel and enrichment in the receiving channel. The direction of the fluid flow for the same applied potential is determined by the choice of pore diameter, pore surface chemistry, channel surface charge, and ionic strength of the buffer. The pores used in this study had a positive surface charge corresponding to negative mobile counter-ions within the pores, while PDMS microchannels had negative surface charge. It was found that for the 200 nm pores the surface charge of the channels dictated the applied voltage that corresponded to forward bias rather than the surface charge of the pores themselves. The opposite was true for an array of 15 nm diameter pores indicating that nanopore EOF dominated in 15 nm pores while channel EOF dominated in 200 nm pores. In such devices, fabrication limitations place constraints on materials and surface properties; however, sizing of the molecular gates can be tuned for desired transport characteristics. Aluru and co-workers (Chatterjee et al. 2005) analyzed the same problem using circuit models to

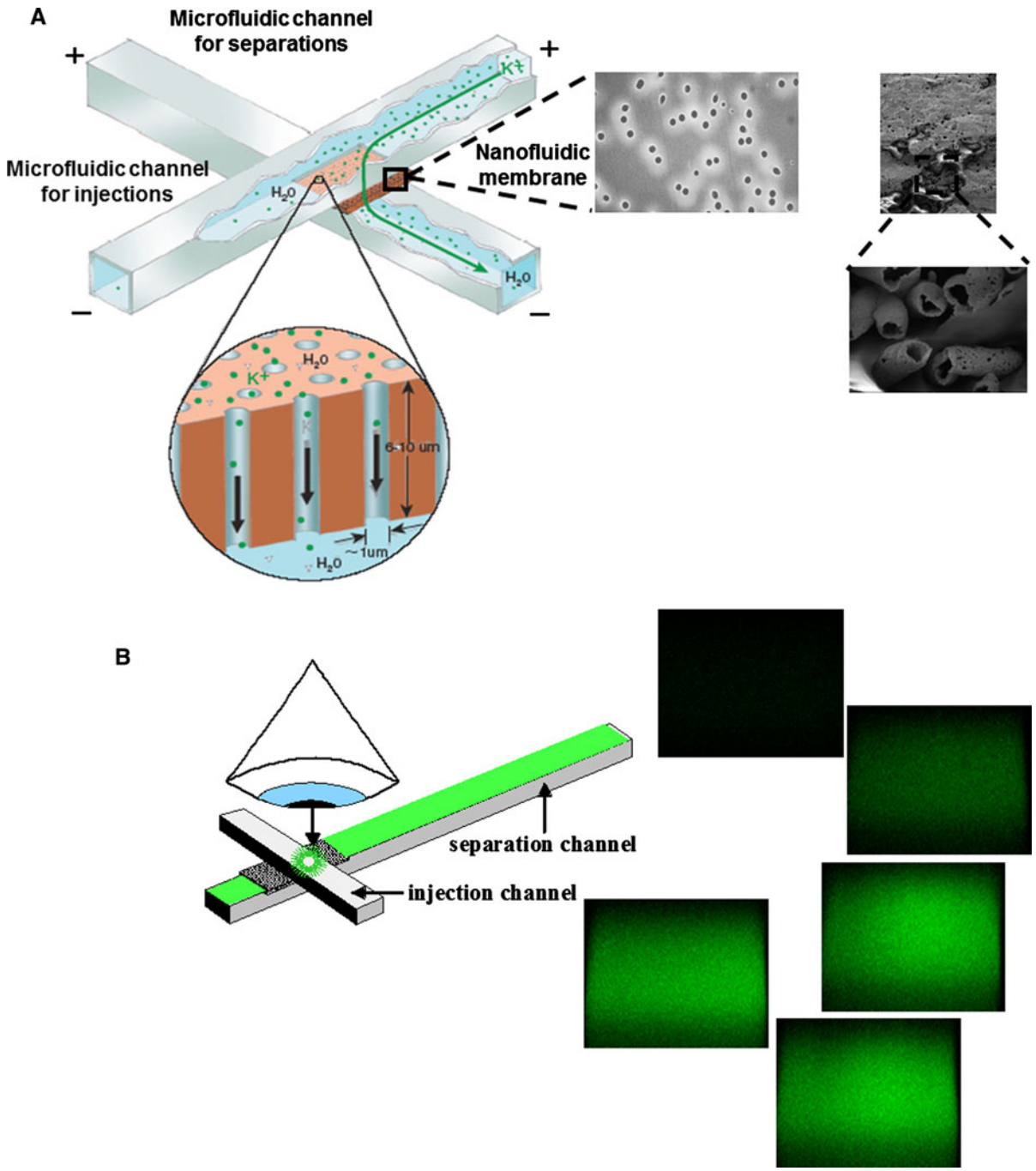

Fig. 3 **a** A schematic for the molecular gate developed using NCAMs. A NCAM with positive surface charge is sandwiched between two PDMS microchannels with negative surface charge, with the inserts showing fluorescence images of the injected samples collected over a period of time. The device is used to illustrate electrically-controlled fluid flow through the NCAM. **b** Demonstrates rapid injection from the source to the receiving channel, with the inserts showing fluorescence images of the injected samples collected over a period of time. Figure from IEEE (Prakash et al. 2008)

determine impedances and calculate ionic currents. The size of the nanopores have a dramatic effect; while, the 200 nm pores contribute as little as 1 % of the total impedance, a 36-fold increase in the case of 15 nm pores highlights the role of nanocapillary EOF in reversing the effective biasing conditions. Subsequently, NCAMs have been integrated within microfluidic devices for quantification of ionic transport regimes (Prakash et al. 2007) and have also been used to develop impedance measurements as a tool.

Switchable fluidic communication in NCAMs used in molecular gates demonstrates diode-like characteristics, with the additional capability of tuning size-dependent fractionation and injection (Kuo et al. 2003a, b). Novel injection strategies have been incorporated for improving peak reproducibility and separation resolution by the use of floating injection methods in NCAM hybrid devices (Gong et al. 2008a, b). Floating injection, albeit lower throughput than the biased injection schemes, addresses non-uniformities in electric field distribution at NCAM-separation channel interfaces to offset issues of broadening and excess injection. The fabrication of such multilayer hybrid microfluidic devices with 3-D NCAM nanofluidic interconnects as molecular gates (Flachsbart et al. 2006) could be used to build lab on a chip (LoC) devices with several stages for multiple unit operations on mass-limited samples.

Transport in metallic NCAMs

Continuously coated Au-NCAMs

Over the last decade there has been increased interest in the use of metal-coated (particularly Au) membranes as a means of extending the range of applications of NCAMs. The motivation stems from the potential for imparting multiple functionalities to the metal-coated membranes: metal-mediated electrokinetic transport in the nanocapillaries (Martin et al. 2001a, b; Lee and Martin 2002; Chun et al. 2006; Buyukserin et al. 2007; Piruska et al. 2008; Piruska et al. 2010a, b), Faradaic electrochemistry (Contento et al. 2011), self-assembly chemistry on coinage metals for specific surface decoration (Chun and Stroeve 2002; Kohli et al. 2004; Huang and Yin 2006; Kim et al. 2007; Jagerszki et al. 2007), and plasmonic behavior when the pores form a translationally symmetric array. Furthermore, these properties can be exploited by itself or in various combinations, for example, using a plasmonic array to sense the change in solution conditions upon carrying out electron transfer reactions.

There are a number of approaches to realizing metallic nanopores. As shown by Martin and co-workers over a decade ago, electroless deposition of thin Au films affords selective control over transport of a range of molecular entities based on their size, charge, and unique chemical properties. Starting from either cylindrical or conical nanopore membranes, simply varying the plating time during electroless deposition enables reproducible fabrication of Au-coated nanopores with varying internal diameters, producing pores as small as several nm in optimal cases (Martin et al. 2001a, b). Elegant experiments using these structures as effective molecular sieves or filters have been described. However, determinations in complex mixtures frequently dictate that additional molecular selection criteria, beyond size exclusion, be employed.

Taking advantage of robust Au-thiol chemistry, Au-coated nanopore surfaces can be functionalized to effect selective passage based on molecular recognition principles. For example, Huang et al. altered the hydrophobicity within Au nanopores using either cysteine or carbamidine terminated thiols to separate tryptophan and vitamin B_2 (Huang and Yin 2006). Au-coated nanopores functionalized with DNA oligonucleotides have been used to capture, and thus selectively retard, complementary strands via DNA hybridization (Jagerszki et al. 2007; Kohli et al. 2004). In addition, the behavior of thiol-terminated Au nanopore modifiers can be conditionally controlled to mediate molecular transport (Chun and Stroeve, 2002). Stroeve and co-workers controllably modulated amino acid transport across Au-NCAMs by varying pH and ionic strength of an electrolyte solution within a nanopore to regulate the structure of the double layer and the charge state of the analyte (Ku et al. 2007).

Modulation of transport is by no means limited to small molecules. Kim et al. immobilized F_{ab}' fragments of anti-insulin in an Au-NCAM using self-assembly through the exposed disulfide. The resulting affinity-NCAM was competent for molecular recognition of its antigen, insulin, as shown by selective release followed by MALDI mass spectrometry (Kim et al. 2007). Finally, as a highly conductive metal, Au

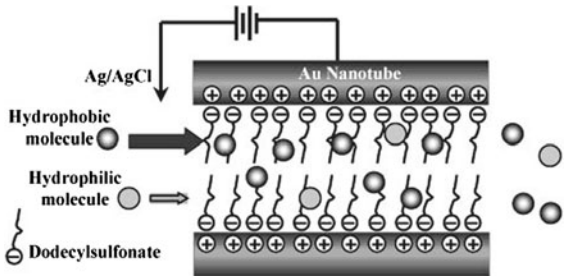

Fig. 4 Surfactant/double layer charging approach for electromodulating neutral molecule transport in Au-NCAMs. Reproduced with permission, (Lee and Martin 2002). Copyright 2002 American Chemical Society

can also be electrostatically charged using an applied potential (Martin et al. 2001a, b), as demonstrated by the electromodulated transport of both small molecules and proteins across Au-NCAMs (Buyukserin et al. 2007; Chun et al. 2006; Lee and Martin 2002). Figure 4 illustrates the strategy: the application of an appropriate electrochemical potential to the Au-coated nanopore results in modulation of the surface density of oppositely charged surfactant molecules, which in turn retard transport of hydrophobic molecules by a mobile-stationary phase partitioning mechanism. Taken together, just this small collection of examples shows how these versatile structures can mimic the behavior of electrophoretic, affinity, and partitioning-based separations used routinely in larger-scale structures.

Partially coated Au-NCAMs

In the previous section, several techniques that have been employed to selectively modulate the diffusive transport of specific molecules across fully coated Au-NCAMs were discussed, but there is a compelling technological motivation for introducing convective transport, in order to significantly improve throughput. However, hydrodynamic strategies employing pressure-driven flow are undesirable for portable applications and are unworkable for pores in the sub-500 nm diameter range, in any case. Furthermore, electrokinetic pumping is limited in continuously coated Au-NCAMs, because the electric fields established by external potentials across these structures are severely distorted by continuous Au layers, thus obviating electrically-controlled transport across these membranes (Piruska et al. 2008). However, NCAMs featuring a thin embedded Au layer are capable of facilitating electrokinetic transport with efficiencies comparable to that of all-dielectric NCAMs (Piruska et al. 2010a, b). Fortunately, NCAM pore dimensions favor rapid EOF driven by applied potentials at the embedded metallic layer of ~ 1 V. Although, injection efficiency across asymmetric NCAMs depends on the orientation of the asymmetric membrane relative to the driving potential, with efficient injections being enabled when the Au coating is on the receiving side of the membrane, reproducible high-quality electrokinetic transport is also achieved in symmetric Au-NCAMs having an embedded gold nanoband region within the nanopores. In addition, embedded Au-layers may serve as working electrodes to drive electrochemical reactions. For example, Contento et al. (2011) reduced water to generate H_2 at nanochannel-embedded electrodes, the hydrogen then being transported by induced electroosmotic flow downstream where it is available for catalytic hydrogenation reactions. Figure 5 depicts the electrochemical generation of H_2 and subsequent transport in planar nanochannels. The abilities discussed here to modulate transport in metallic NCAMs based on molecular recognition and to carry out reactive processing emphasize the fact that nanoband Au-NCAMs are excellent candidates for a range of applications, including high-efficiency electrochemical sensing, electrochemically catalyzed conversion, or pretreatment and label free sensing utilizing extraordinary optical transmission based plasmonic responses.

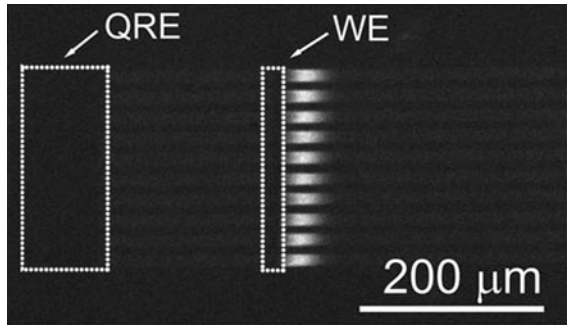

Fig. 5 Generation of H_2 within nanochannel arrays at working electrode (WE), evidenced by an increase in fluorescein indicator fluorescence caused by the rise in pH, and electroosmotic transport downstream (*left* to *right*) by electric field established between the embedded working and quasi-reference (QRE) electrodes. Reproduced from (Contento et al. 2011), by permission of The Royal Society of Chemistry

Applications

Transport through nanostructures has allowed many interesting and innovative applications such as fluidic transistors and diodes, rapid fluid injections, high-throughput reactions, separations, sample mixing, sample concentrating, filtering and sieving, and molecular gating as discussed in detail below. Several of these unit operations can be combined on a single platform to create a micro-total analysis (μ-TAS) system or LoC.

Fundamental studies

NCAMs have been used since the early 1990s to conduct a variety of studies for probing fundamentals of confined nanofluidic transport. Such studies were enabled by the relatively monodisperse pore size distribution achieved during the alpha particle tracking and subsequent etching to make the NCAMs. Initial studies evaluated perm selectivity of ionic species due to surface charge shielding as a function of Debye length (Kemery et al. 1998; Kuo et al. 2001; Nishizawa et al. 1995; Lee and Martin 2002; Jirage et al. 1999; Martin et al. 2001a, b; Hulteen et al. 1998). In the last 5 years or so, as the overall knowledge base for nanofluidic transport phenomena has grown, NCAMs have been integrated within model systems to predict geometry of nanocapillaries using impedance measurements (Vitarelli et al. 2011), to study redox activity of surface functional groups and enhanced transport through nanopores using cyclic voltammetry (CV) (Perera and Ito 2010), and also for studies of electric field mediated wetting phenomena (Powell et al. 2011).

Sample injection/separation

An NCAM sandwiched between two microfluidic channels can be used to electrokinetically inject samples from a source microchannel to a separation microchannel, where electrophoretic separations are performed (see Fig. 3b). Initially a potential is applied across the separation channel with the waste reservoir of the separation channel grounded. During this step the source channel is allowed to float. A picoliter volume from the source side is injected through the NCAM by applying equal potential to either side of the source channel and grounding the waste reservoir of the separation channel. This results in the injection of a well-defined sample plug into the separation channel. Injection times are short, typically a few hundred ms. Electrophoretic separation is then performed on the sample plug before another sample injection (Cannon et al. 2003). This design can also be adapted for sample collection. If a third channel is added and separated by an NCAM from the separation channel, following injection the sample plug can be transferred down the separation channel by electroosmosis and then collected in the third channel by applying an equal bias to both reservoirs of the separation channel and grounding the collection channel (Kuo et al. 2003a, b). These studies illustrate the ability to manipulate flows of mass-limited samples (Shannon et al. 2005; Tulock et al. 2004). The transport of target molecules through NCAMs can be controlled by ionic strength, magnitude, and polarity of the applied potential, pore size, and surface chemistry (i.e., surface charge density and surface energy). NCAMs allow for electrically-controlled valving and rapid sample injections (Wernette et al. 2006; Gong et al. 2008a, b; Wang et al. 2009) with high-sample plug reproducibility, and separation resolution, and reproducibility approaching 1 % for some studies (Cannon et al. 2003). Following the success of these initial demonstrations of molecular gates, new planar microchannel–nanochannel hybrid devices have been developed that allow for controlled dosing of a variety of transfection agents to single cells through electroporation at the microchannel–nanochannel interface (Boukany et al. 2011) with potential applications in high-throughput drug delivery.

Similar injection/collection strategies have been implemented to perform two-stage sample separation. The first stage is electrophoretic separation based on electrophoretic mobilities of varying species, while the second stage involving chiral amino acid mixture separation is achieved through micellar electrokinetic chromatography with a chiral selector. Separation depends critically on injection and collection capabilities in the device. Such separations are important to biochemical studies that require the separation of complex mixtures of analytes with orthogonal separation principles (Kim et al. 2009).

Sieving/filtration

Nanoscale structures such as nanopores and nanochannels allow for the fabrication of molecular filters

of sieves since the size of many biomolecules is on the same order as the characteristic size of these structures themselves. Transport through pores is affected by steric hindrance or exclusion due to molecular entropy, hydrodynamic hindrance, caused by viscous forces associated with the walls of the pores, and charge interactions between the molecule and the surface of the nanopore or nanochannel. Molecules that are larger than the size of the pores themselves can be electrically driven through the pore forcing the molecules to change their shape and conformation. Pore/channel size, surface chemistry (i.e., charge), applied potentials, and multi-step filtrations with different membranes can be used to perform highly efficient separations (Yan et al. 2009; Karnik et al. 2006). Furthermore, methods for active manipulation of the pore geometry using stimulus-responsive polymers, through temperature-mediated shape changes in polymer brushes (Lokuge et al. 2007) and pressure-induced insertion of ion-channels in lipid bilayers (Schibel et al. 2011), have been demonstrated that permit actively-controlled size-selective transport across NCAMs.

Rapid reagent mixing

Incorporating NCAMs into microfluidic structures affords a highly tunable, nanoscale pathway for the transport of molecules from one chemical environment to another (Fa et al. 2005). Typically 5–50 μm thick, NCAMs support rapid electroosmotic flow with relatively low-electrical potentials. Under such conditions linear velocities of order $\sim$1 mm s^{-1} can be achieved across the nanopore. In addition, permitting the digital switching of fluid packets across the nanopores, and coupling of rapid flow in the nanopores to the microfluidic channels feeding those results in advantageous mixing behavior, as well. In general, electrokinetic transport in microfluidic channels occurs at low Reynolds number (10^{-3}–10^{-2}), and as a result, mixing of molecular entities across streamlines relies on Fickian diffusion. However, nanochannel mediated electroosmotic flow encourages convective mixing at the micro/nanochannel junction, as demonstrated by effective mixing within 3D structures comprised of orthogonal microfluidic channels surrounding a polymeric NCAM (Kuo et al. 2004). This strategy has been successfully used for injecting Ca^{2+} into a channel containing a fluorogenic Ca^{2+} probe or molecular beacon action by introducing Pb^{2+} into a channel containing a DNA aptazyme, which is quenched in its native state but unquenched after analyte-mediated dehybridization (Chang et al. 2005). Similarly, large biomolecules, such as enzymes suspended in a microfluidic channel can be electrokinetically injected across an NCAM into an orthogonal microchannel containing the substrate, where the two entities convectively mix and react at the nanopore/microchannel junction (Gong et al. 2008a, b). These operations, which exploit the rapid response to control signal for electrokinetic transport and rapid mixing, mimic the behavior of stopped-flow reactors, but on volumes that are orders of magnitude smaller than bench-top stopped-flow instruments.

Analyte pre-concentration

NCAMs integrated into microfluidic devices can be used to pre-concentrate the sample before injecting it through the NCAM. In one demonstration, fluorescein, a negatively charged dye, was combined with a buffer solution. A positive potential was applied to the source side of the device while the receiving side (other side of NCAM) was grounded. The fluorescein dye was repelled away from the positive electrode and collected on the source side of the NCAM. The surface of the NCAM was positively charged corresponding to negative mobile counter-ions in the pores. This prevented fluorescein from simply passing through the pore for the initial voltage configuration. The dye collected near the NCAM after 40 min was 300 times the initial concentration of the fluorescein for both 1 μM or 0.1 μM initial concentrations, indicating that the concentration was independent of the repulsive forces between the fluorescein molecules (Zhang and Timperman 2003). When the bias was reversed, the pre-concentrated sample was transported through the NCAM to the receiving side. Pre-concentration has applications in biochemical studies where small amounts of biomolecules can be pre-concentrated before detection, allowing lower detection limits. Studies have used techniques based on pre-concentration in a T-shaped device for pre-concentration of DNA (Khandurina et al. 1999).

One interesting phenomenon that takes place at the micro-nanochannel interface is that of concentration polarization, with one end being enriched and the other depleted for a given species (Piruska et al. 2010a, b).

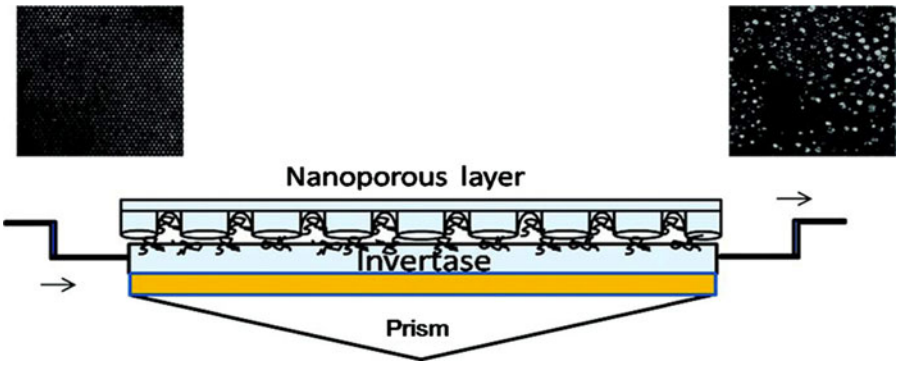

Fig. 6 Flow cell to monitor real-time production of glucose and fructose. Substrate (sucrose) is introduced convectively to nanoporous anodic alumina featuring immobilized invertase from left to right. Sucrose/invertase interaction is monitored by surface plasmon resonance (SPR) measurement. Reproduced with permission, (Dhathathreyan 2011). Copyright 2011 American Chemical Society

Gradients in ionic concentration cause added impedance to solute rejection, and the resulting concentration polarization serves as a limiting factor for water flux through reverse osmosis membranes. Bio-inspired systems are envisaged for energetically favorable pumping of hydrated ions through membranes by modulating pore potentials (Shannon et al. 2008). The phenomenon of concentration polarization, in combination with pressure-driven flow, has also been used to create ion and particle depletion zones around membranes to develop devices for water desalination (Kim et al. 2010). Similar strategies exploiting the space-charge region at the microfluidic-nanofluidic interface have shown concentration polarization factors in excess of 10^6 (Wang et al. 2005).

Improved enzyme reaction kinetics

With pore dimensions as small as several nanometers, the fluid transport properties of NCAMs differ considerably from those in microfluidic structures. In particular, lateral (radial) diffusion can efficiently deliver molecules from the center of the channel to the walls at the nanoscale and, thus, can effectively be combined with electrokinetically-driven axial flow. Applications employing nanochannel-immobilized enzymes are particularly attractive. With relatively short distances for substrates to traverse, it is expected that they will encounter surface-bound enzymes many times during transit through the nanochannel, thereby rendering enzyme kinetics within confined geometries superior to those in bulk solution (Dhathathreyan 2011). Figure 6 illustrates the immobilization of the enzyme, invertase, onto a nanoporous membrane for the conversion of sucrose into glucose and fructose. The flow cell device used in this study not only exhibits a higher rate of enzyme/substrate interaction than in bulk (Bowski et al. 1971), but also requires a lower substrate concentration for product detection. In another study, reaction–diffusion modeling was combined with measurements of enzymatic reaction velocities during injection-relaxation cycles across an NCAM to show that the enzymatic activity of immobilized horseradish peroxidase in NCAMs is up to 10^2 times higher than in free solution (Wang et al. 2009). Most notably, electrokinetic transport in NCAMs affords rapid convective delivery of substrates to active sites to improve turnover of mass transport limited enzymatic reactions. Thus, enzyme-functionalized NCAMs utilized within microfluidic devices, as described above, show great promise for in situ generation of biological reagents for downstream reactions.

Sensors

There is a growing interest in portable detection devices that can perform complete measurements including sample manipulation and detection in a matter of minutes using increasingly smaller sample volumes approaching the picoliter or smaller sample volumes, especially for point-of-use applications. Nanopores and nanofluidic devices allow for manipulation of such small sample volumes. Several sensors based on nanopores have been developed, for example one for hydrogen peroxide (Ali et al. 2011). Furthermore, a transducer can be integrated directly into a nanofluidic

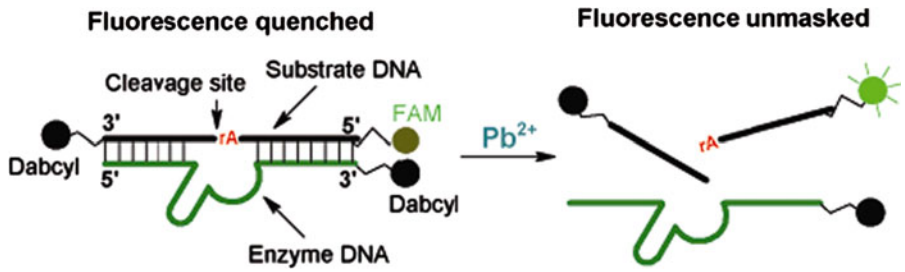

Fig. 7 Sensing using dehybridization reactions of DNAzyme immobilized inside NCAMs. FAM fluorescence from the substrate is initially suppressed by Dabcyl quencher on the enzyme. Cleavage of DNA in the presence of Pb^{2+} releases fluorescent product for subsequent detection. Reproduced with permission, (Chang et al. 2005). Copyright 2005 American Chemical Society

device, for the detection of either biomolecules such as proteins and nucleic acids or heavy metal contaminants in water (Prakash et al. 2012a, b). A further demonstration of the utility of carrying out molecular recognition reactions in nanopores utilizes the catalytic DNA molecular beacon introduced above. Catalytic DNA molecules, or DNAzymes, facilitate multiple turnover reactions (Lu and Liu 2006), but in this chemical sensing application the enzyme strand facilitates recognition of the analyte that occurs on the complementary substrate strand. Figure 7 illustrates the operating principle, in which Pb^{2+}-mediated cleavage of DNA leads to the release of the FAM conjugate. FAM fluorescence, originally quenched by Dabcyl, is enhanced by orders of magnitude upon dehybridization. Recognition reactions are most frequently implemented as homogeneous reactions, however it was discovered that immobilization of DNAzymes within NCAMs greatly enhanced sensitivity and lowered limits of detection—a promising strategy for biosensing applications (Adiga et al. 2009). In addition to the potential in vivo detectors, DNAzyme functionalized NCAMs have been incorporated into microfluidic devices for real-time detection of harmful toxins (Chang et al. 2005; Wernette et al. 2006).

Fluidic transistors and diodes

Nanofluidic channels and nanopores allow for ion transport manipulation that parallels electronic devices such as field effect transistors (FETs) (Nam et al. 2009) and diodes (Yan et al. 2009). The ability to control charge movement is due to the fact that the characteristic length of the channel is on the same order as the size of the EDL. An applied potential across the length of a channel drives an electroosmotic flow. A perpendicular electric field is created by controlling the surface charge through a third electrode on the channel wall. The magnitude of this electric field serves to increase, decrease or even reverse the EOF velocity (Karnik et al. 2005; Schasfoort et al. 1999; Kuo et al. 2003a, b). These devices are known as flow FETs. Such devices have been used for selective protein transport allowing for manipulation of biomolecules in picoliter size samples (Karnik et al. 2006). A nanofluidic channel that has a surface charge of equivalent magnitude but opposite polarity on the left and right halves of the channel can serve as a fluidic diode, allowing electrolyte to pass under forward bias but blocking flow during reverse bias as long as the double layers do not overlap (Daiguji et al. 2005; Vlassiouk and Siwy 2007). Recently, tunable transport characteristics and diode-behavior have been demonstrated in NCAMs through induced charge inversion (He et al. 2009) and electrostatic gating (Pardon and van der Wijngaart 2011).

Summary

Nanofluidic systems that combine NCAMs and microfluidic elements benefit from physical phenomena interacting on multiple length scales. NCAMs with microfluidics exploit the role of surface properties and geometric characteristics that govern physical phenomena, such as molecular diffusion and electrostatic forces, and electrokinetic effects arising from their coupling with physical device dimensions. While ongoing fundamental studies continue to refine the

state-of-art in understanding nanofluidic transport, our growing ability to create well-defined periodic nanometer scale capillary arrays, define their surface functionality, and address them in ways to separate diverse chemical environments and control fluidic communication between them have enabled experiments using NCAMs to mimic biological membrane processes. Advancements from the last decade have brought us a step closer to realizing systems capable of manipulating molecules one-by-one, thus affording processes of extraordinary power for chemical sensing, analysis, separation, and energy conversion.

Acknowledgments Mark Shannon and Vikhram Swaminathan acknowledge support through WaterCAMPWS, Center for Advanced Materials for the Purification of Water with Systems, a US National Science Foundation funded Science and Technology Center under contract CTS-0120978, and the US Defense Advanced Research Projects Agency under grant W911NF-09-C-0079. The portion of this study conducted at the University of Notre Dame was supported by the US National Science Foundation under grants DBI 0852741 and CBET 0120978, by the US Department of Energy Office of Basic Energy Sciences DE FG02 07ER15851, and by the US Army Corps of Engineers contract W9132-10-0010. Shaurya Prakash and Marie Pinti acknowledge partial support through the US Defense Advanced Research Projects Agency grant W911NF-09-C-0079.

References

Adiga SP, Jin CM, Curtiss LA, Monteiro-Riviere NA, Narayan RJ (2009) Nanoporous membranes for medical and biological applications. WIREs Nanomed Nanobiotechnol 1:568–581

Agerbaek M, Keiding K (1995) Streaming potential during cake filtration of slightly compressible particles. J Colloid Interface Sci 169:255–342

Ali M, Tahir MN, Siwy ZS, Neumann R, Tremel W, Ensinger W (2011) Hydrogen peroxide sensing with horseradish peroxidase-modified polymer single conical nanochannels. Anal Chem 83:1673–1680

Bohn PW (2009) Nanoscale control and manipulation of molecular transport in chemical analysis. Annu Rev Anal Chem 2:279–296

Boukany PE, Morss A, Liao W, Henslee B, Jung H, Zhang X, Yu B, Wang X, Wu Y, Li L, Gao K, Hu X, Zhao X, Hemminger O, Lu W, Lafyatis GP, Lee LJ (2011) Nanochannel electroporation delivers precise amounts of biomolecules into living cells. Nat Nanotechnol 6:747–754

Bowski L, Saini R, Ryu D, Vieth W (1971) Kinetic modeling of hydrolysis of sucrose by invertase. Biotechnol Bioeng 13:641–656

Burgmayer P, Murray RW (1982) An ion gate membrane: electrochemical control of ion permeability through a membrane with an embedded electrode. J Am Chem Soc 4:6139–6140

Burgreen D, Nakache F (1964) Electrokinetic flow in ultrafine capillary slits. J Phys Chem 68:1084–1091

Buyukserin F, Kohli P, Wirtz M, Martin C (2007) Electroactive nanotube membranes and redox-gating. Small 3:266–270

Cannon DM Jr, Kuo T-C, Bohn PW, Sweedler JV (2003) Nanocapillary array interconnects for gated analyte injections and electrophoretic separations in multilayer microfluidic architectures. Anal Chem 75:2224–2230

Cervera J, Patricio R, Manzanares JA, Mafe S (2010) Incorporating ionic size in the transport equations for charged nanopores. Microfluid Nanofluid 9:41–53

Chang I-H, Tulock JJ, Liu J, Cannon DM Jr, Bohn PW, Sweedler JV, Cropeck DM (2005) Miniaturized lead sensor based on lead-specific DNAzyme in a nanocapillary interconnected microfluidic device. Environ Sci Technol 39:3756–3761

Chatterjee AN, Cannon DM Jr, Gatimu EN, Sweedler JV, Aluru NR, Bohn PW (2005) Modeling and simulation of ionic currents in three-dimensional microfluidic devices with nanofluidic interconnects. J Nanopart Res 7:507–516

Chowdiah P, Wasan D, Gidaspow D (1983) On the interpretation of streaming potential data in nonaqueous media. Colloids Surf 7:291–299

Chun K-Y, Stroeve P (2002) Protein transport in nanoporous membranes modified with self-assembled monolayers of functionalized thiols. Langmuir 18:4653–4658

Chun K-Y, Mafe S, Ramirez P, Stroeve P (2006) Protein transport through gold-coated, charged nanopores: Effects of applied voltage. Chem Phys Lett 418:561–564

Conlisk AT (2005) The Debye-Huckel approximation: Its use in describing electroosmotic flow in micro- and nanochannels. Eletrophoresis 26:1896–1912

Conlisk AT (2012) Essentials of micro- and nanofluidics: with applications to the biological and chemical sciences. Cambridge University Press, Cambridge

Conlisk AT, McFerran J, Zheng Z, Hansford D (2002) Mass transfer and flow in electrically charged micro- and nanochannels. Anal Chem 74:2139–2150

Conlisk AT, Kumar A, Rampersaud A (2007) Ionic and biomolecular transport in nanochannels. Nanoscale Microscale Thermophys Eng 11:177–199

Contento NM, Branagan SP, Bohn PW (2011) Electrolysis in nanochannels for in situ reagent generation in confined geometries. Lab Chip 11:3634–3641

Daiguji H, Oka Y, Shirono K (2005) Nanofluidic diode and bipolar transistor. Nano Lett 5:2274–2280

Datta S, Conlisk AT, Kanani DM, Zydney AL, Fissell WH, Roy S (2010) Characterizing the surface charge of synthetic nanomembranes by the streaming potential method. J Colloid Interface Sci 348:85–95

Dhathathreyan A (2011) Real-time monitoring of invertase activity immobilized in nanoporous aluminum oxide. J Phys Chem B 115:6678–6682

Fa K, Tulock JJ, Sweedler JV, Bohn PW (2005) Profiling pH gradients across nanocapillary array membranes connecting microfluidic channels. J Am Chem Soc 127:13928–13933

Fievet P, Szymczyk A, Aoubiza B, Pagetti J (2000) Evaluation of three methods for the characterisation of the membrane-solution interface: streaming potential, membrane potential and electrolyte conductivity inside pores. J Membr Sci 168:87–100

Flachsbart BR, Wong K, Iannacone JM, Abante EN, Vlach RI, Rauchfuss PA, Bohn PW, Sweedler JV, Shannon MA (2006) Design and fabrication of a multilayered polymer microfluidic chip with nanofluidic interconnects via adhesive contact printing. Lab Chip 6:667–674

Gong M, Flachsbart BR, Shannon MA, Bohn PW, Sweedler JV (2008a) Fluidic communication between multiple vertically segregated microfluidic channels connected by nanocapillary array membranes. Electrophoresis 29:1237–1244

Gong M, Kim BY, Flachsbart BR, Shannon MA, Bohn PW, Sweedler JV (2008b) An on-chip fluorogenic enzyme assay using a multilayer microchip interconnected with a nanocapillary array membrane. IEEE Sens J 8:601–607

Han J, Fu J, Schoch RB (2008) Molecular sieving using nanofilters: past, present and future. Lab Chip 8:23–33

He Y, Gillespie D, Boda D, Vlassiouk I, Eisenberg RS, Siwy ZS (2009) Tuning transport properties of nanofluidic devices with local charge inversion. J Am Chem Soc 131:5194–5202

Huang S, Yin Y (2006) Transport and separation of small organic molecules through nanotubules. Anal Sci 22:1005–1009

Huisman IH, Pradanos P, Calvo JI, Hernandez A (2000) Electroviscous effects, streaming potential, and zeta potential in polycarbonate track-etched membranes. J Membr Sci 178: 79–92

Hulteen JC, Jirage KB, Martin CR (1998) Introducing chemical transport selectivity into gold nanotubule membranes. J Am Chem Soc 120:6603–6604

Jagerszki G, Gyurcsanyi R, Hofler L, Pretsch E (2007) Hybridization-modulated ion fluxes through peptide-nucleic-acid-functionalized gold nanotubes. A new approach to quantitative label-free DNA analysis. Nano Lett 7:1609–1612

Jirage KB, Hulteen JC, Martin CR (1999) Effect of thiol chemisorption on the transport properties of gold nanotubule membranes. Anal Chem 71:4913–4918

Karnik R, Fan R, Yue M, Li D, Yang P, Majumdar A (2005) Electrostatic control of ions and molecules in nanofluidic transistors. Nano Lett 5:943–948

Karnik R, Castelino K, Majumdar A (2006) Field-effect control of protein transport in a nanofluidic transistor circuit. Appl Phys Lett 88:123114

Kemery PJ, Steehler JK, Bohn PW (1998) Electric field mediated transport in nanometer diameter channels. Langmuir 14:2884–2889

Khandurina J, Jacobson SC, Waters LC, Foote RS, Ramsey JM (1999) Microfabricated porous membrane structure for sample concentration and electrophoretic analysis. Anal Chem 71:1815–1819

Kim BY, Swearingen CB, Ho JA, Romanova EV, Bohn PW, Sweedler JV (2007) Direct immobilization of Fab' in nanocapillaries for manipulating mass-limited samples. J Am Chem Soc 129:7620–7626

Kim BY, Yang J, Gong M, Flachsbart BR, Shannon MA, Bohn PW, Sweedler JV (2009) Multidimensional separation of chiral amino acid mixtures in a multilayered three-dimensional hybrid microfluidic/nanofluidic device. Anal Chem 81:2715–2722

Kim S, Ko S, Kang K, Han J (2010) Direct seawater desalination by ion concentration polarization. Nat Nanotechnol 5: 297–301

Kohli P, Harrell CC, Cao Z, Gasparac R, Tan W, Martin CR (2004) DNA-functionalized nanotube membranes with single-base mismatch selectivity. Science 305:984–986

Ku J-R, Lai S-M, Ileri N, Ramirez P, Mafe S, Stroeve P (2007) pH and ionic strength effects on amino acid transport through Au-nanotubule membranes charged with self-assembled monolayers. J Phys Chem C 111:2965–2973

Kuo T-C, Sloan LA, Sweedler JV, Bohn PW (2001) Manipulating molecular transport through nanoporous membranes by control of electrokinetic flow- effect of surface charge density and Debye length. Langmuir 17:6298–6303

Kuo T-C, Cannon DM Jr, Chen Y, Tulock JJ, Shannon MA, Sweedler JV, Bohn PW (2003a) Gateable nanofluidic interconnects for multilayered microfluidic separation systems. Anal Chem 75:1861–1867

Kuo T-C, Cannon DM Jr, Shannon MA, Bohn PW, Sweedler JV (2003b) Hybrid three-dimensional nanofluidic/microfluidic devices using molecular gates. Sens Actuators, A 102: 223–233

Kuo T-C, Kim H-K, Cannon DM Jr, Shannon MA, Sweedler JV, Bohn PW (2004) Nanocapillary arrays effect mixing and reaction in multilayer fluidic structures. Angew Chem 116:1898–1901

Lee SB, Martin CR (2002) Electromodulated molecular transport in gold-nanotube membranes. J Am Chem Soc 124: 11850–11851

Lokuge I, Wang X, Bohn PW (2007) Temperature-controlled flow switching in nanocapillary array membranes mediated by poly(*N*-isopropylacrylamide) polymer brushes grafted by atom transfer radical polymerization. Langmuir 23: 305–311

Lu Y, Liu J (2006) Functional DNA nanotechnology: emerging applications of DNAzymes and aptamers. Curr Opin Biotechnol 17:580–588

Martin CR, Nishizawa M, Jirage K, Kang MS, Lee SB (2001a) Controlling ion-transport selectivity in gold nanotubule membranes. Adv Mater 13:1351–1362

Martin CR, Nishizawa M, Jirage K, Kang M (2001b) Investigations of the transport properties of gold nanotubule membranes. J Phys Chem B 105:1925–1934

Mulero R, Prabhu AS, Freedman KJ, Kim MJ (2010) Nanopore-based devices for bioanalytical applications. JALA 15: 243–252

Nam S-W, Rooks MJ, Kim K-B, Rossnagel SM (2009) Ionic field effect transistors with sub-10 nm multiple nanopores. Nano Lett 9:2044–2048

Napoli M, Eijkel J, Pennathur S (2010) Nanofluidic technology for biomolecule applications: a critical review. Lab Chip 10:957–985

Nishizawa M, Menon VP, Martin CR (1995) Metal nanotubule membranes with electrochemically switchable ion-transport selectivity. Science 268:700–702

Nystrom M, Lindstrom M, Matthiasson E (1989) Streaming potential as a tool in the characterization of ultrafiltration membranes. Colloids Surf 36:297–312

Oukhaled A, Cressiot B, Bacri L, Pastoriza-Gallego M, Betton J-M, Bourhis E, Jede R, Gierak J, Auvray L, Pelta J (2011) Dynamics of completely unfolded and native proteins

through solid-state nanopores as a function of electric driving force. ACS Nano 5:3628–3638

Pardon G, van der Wijngaart W (2011) Electrostatic gating of ion and molecule transport through a nanochannel-array membrane. Proc IEEE Solid-State Sens Actuators Microsyst Conf (Transducers) Beijing, China, pp 1610-1613

Perera DNT, Ito T (2010) Cyclic voltammetry on recessed nanodisk-array electrodes prepared from track-etched polycarbonate membranes with 10-nm diameter pores. Analyst 135:172–176

Piruska A, Branagan SP, Cropek DM, Sweedler JV, Bohn PW (2008) Electrokinetically driven fluidic transport in integrated three-dimensional microfluidic devices incorporating gold-coated nanocapillary array membranes. Lab Chip 8:1625–1631

Piruska A, Branagan SP, Minnis AB, Wang Z, Cropeck DM, Sweedler JV, Bohn PW (2010a) Electrokinetic control of fluid transport in gold-coated nanocapillary array membranes in hybrid nanofluidic-microfluidic devices. Lab Chip 10:1237–1244

Piruska A, Gong M, Sweedler JV, Bohn PW (2010b) Nanofluidics in chemical analysis. Chem Soc Rev 39:1060–1072

Plecis A, Schoch RB, Renaud P (2005) Ionic transport phenomena in nanofluidics: experimental and theoretical study of the exclusion-enrichment effect on a chip. Nano Lett 5:1147–1155

Powell MR, Cleary L, Davenport M, Shea KJ, Siwy ZS (2011) Electric-field-induced wetting and dewetting in single hydrophobic nanopores. Nat Nanotechnol 6:798–802

Prakash S, Yeom J, Jin N, Adesida I, Shannon MA (2007) Characterization of ionic transport at the nanoscale. Proc ASME IMECE, N: J Nanoeng Nanosyst 220:45–52

Prakash S, Piruska A, Gatimu EN, Bohn PW, Sweedler JV, Shannon MA (2008) Nanofluidics: Systems and Applications. IEEE Sens J 8:441–450

Prakash S, Karacor M, Benerjee S (2009) Surface modification in microsystems and nanosystems. Surf Sci Rep 64: 233–254

Prakash S, Pinti M, Bellman K (2012a) Variable cross-section nanopores fabricated in silicon nitride membranes using a transmission electron microscope. J Micromech Microeng in press

Prakash S, Pinti M, Bhushan B (2012b) Theory, fabrication and applications of microfluidic and nanofluidic biosensors. Philos Trans R Soc London, Ser A 370:2269–2303

Qiao R, Aluru N (2003) Ion concentration and velocity in nanochannel electroosmotic flows. J Chem Phys 118: 4692–4701

Qiao R, Aluru N (2004) Charge inversion and flow reversal in a nanochannel electroosmotic flow. Phys Rev Lett 92: 198301

Qiao R, Georgiadis J, Aluru N (2006) Differential ion transport induced electroosmosis and internal recirculation in heterogeneous osmosis membranes. Nano Lett 6:995–999

Renkin E (1954) Filtration, diffusion, and molecular sieving through porous cellulose membranes. J Gen Physiol 38: 225–243

Rice C, Whitehead R (1965) Electrokinetic flow in a narrow cylindrical capillary. J Phys Chem 69:4017–4024

Sadr R, Yoda M, Gnanaprakasam P, Conlisk AT (2006) Velocity measurements inside the diffuse electric double layer in electro-osmotic flow. Appl Phys Lett 89:044103

Schasfoort RB, Schlautmann S, Hendrikse J, van den Berg A (1999) Field-effect flow control for microfabricated fluidic networks. Science 286:942–944

Schibel AE, Heider EC, Harris JM, White HS (2011) Fluorescence microscopy of the pressure-dependent structure of lipid bilayers suspended across conical nanopores. J Am Chem Soc 133:7810–7815

Schoch RB, Han J, Renaud P (2008) Transport phenomena in nanofluidics. Rev Mod Phys 80:839–883

Shannon MA, Flachsbart BR, Iannacone JM, Wong K, Cannon Jr DM, Fa K, Sweedler JV, Bohn PW (2005) Nanofluidic interconnects within a multilayer microfluidic chip for attomolar biochemical analysis and molecular manipulation. Proc 3rd Ann IEEE Int EMBS Special Topic Conf Microtechnol Medicine Biology Kahuhu, pp 257-259

Shannon MA, Bohn PW, Elimelech M, Georgiadis JG, Marinas BJ (2008) Science and technology for water purification in the coming decades. Nature 452:301–310

Sparreboom W, van den Berg A, Eijkel J (2009) Principles and applications of nanofluidic transport. Nat Nanotechnol 4: 713–720

Sparreboom W, van den Berg A, Eijkel J (2010) Transport in nanofluidic systems: a review of theory and applications. New J Phys 12:015004

Szymczyk A, Aoubiza B, Fievet P, Pagetti J (1999) Electrokinetic phenomena in homogeneous cylindrical pores. J Colloid Interface Sci 216:285–296

Talaga DS, Li J (2009) Single-Molecule Protein Unfolding in Solid State Nanopores. J Am Chem Soc 131:9287–9297

Tulock JJ, Shannon MA, Bohn PW, Sweedler JV (2004) Microfluidic Separation and Gateable Fraction Collection for Mass-Limited Samples. Anal Chem 76:6419–6425

Vitarelli M, Prakash S, Talaga D (2011) Determining nanocapillary geometry from electrochemical impedance spectroscopy using a variable topology network circuit model. Anal Chem 83:533–541

Vlassiouk I, Siwy ZS (2007) Nanofluidic diode. Nano Lett 7: 552–556

Wang Y-C, Stevens A, Han J (2005) Million-fold preconcentration of proteins and peptides by nanofluidic filter. Anal Chem 77:4293–4299

Wang Z, King TL, Branagan SP, Bohn PW (2009) Enzymatic activity of surface-immobilized horseradish peroxidase confined to micrometer- to nanometer-scale structures in nanocapillary array membranes. Analyst 134:851–859

Wernette DP, Swearingen CB, Cropek DM, Lu Y, Sweedler JV, Bohn PW (2006) Incorporation of a DNAzyme into Au-coated nanocapillary array membranes with an internal standard for Pb(II) sensing. Analyst 131:41–47

Yan R, Liang W, Fan R, Yang P (2009) Nanofluidic diodes based on nanotube heterojunctions. Nano Lett 9:3820–3825

Zhang Y, Timperman AT (2003) Integration of nanocapillary arrays into microfluidic devices for use as analyte concentrators. Analyst 128:537–542